Interaction of a glucuronoyl esterase with complex fragments of the plant cell wall hemicellulose

International Journal of Biological Macromolecules 352 (2026) 151020

Contents lists available at ScienceDirect

International Journal of Biological Macromolecules

journal homepage: www.elsevier.com/locate/ijbiomac

Interaction of a glucuronoyl esterase with complex fragments of the plant cell wall hemicellulose

A. Zaghini [a,1,2], E.B. Østberg [a,2], S. Banerjee [a], S. Mazurkewich [b], L. Yu [c], P. Dupree [c], J. Larsbrink [b], L. Lo Leggio [a,*]

[a] Department of Chemistry, University of Copenhagen, DK-2100, Copenhagen, Denmark
[b] Wallenberg Wood Science Center, Department of Life Sciences, Chalmers University of Technology, SE-412 96, Gothenburg, Sweden
[c] Department of Biochemistry, University of Cambridge, Cambridge, CB2 1QW, UK

ARTICLE INFO

Keywords:
Decorated polysaccharides
Hemicellulose
Lignin-carbohydrate complex
Lignocellulose
Crystal structure
Carbohydrate esterase

ABSTRACT

Glucuronoyl esterases (GEs) catalyze the cleavage of ester linkages between lignin and glucuronic acid moieties on glucuronoxylan in plant cell walls and are promising biochemical tools for industrial processing of these recalcitrant natural resources. However, details on how GEs interact with and catalyze degradation of their natural substrates are sparse. Using well-diffracting crystals of the model GE *Ot*CE15A, we sought to structurally elucidate its interactions with fragments and analogues of the lignin carbohydrate complex, including commercially available oligosaccharides, digests of complex polysaccharides, and chemical fragments representing building blocks of lignin. While most compounds failed to bind in crystals, the analysis uncovered the structure of a complex with a heptasaccharide (a decorated xylopentaose), the largest ligand bound to a GE experimental structure to date. Most hydrogen bonding interactions are with the glucuronic acid moiety, which is almost totally buried upon binding; however, the rest of the saccharide chain also has a significant contact surface. The structure shows for the first time that *Ot*CE15A can accommodate an arabinose decoration on the glucuronoxylan chain it attacks. Structural comparison suggests that the polysaccharide conformation may influence specificity, reinforcing the view of GEs as true carbohydrate-active enzymes rather than opportunistic promiscuous esterases.

1. Introduction

Lignocellulose is an abundantly available bio-resource with an annually worldwide production around 10–50 billion tons, in dry weight [1]. The utilization of lignocellulosic side-streams and waste biomasses for the production of renewable energy carriers, such as bioethanol, or as a building block for materials and fine chemicals increases the value chain of biorefineries by lowering disposal costs, and it furthermore represents an alternative to products derived from fossil fuels [2]. Valorisation of lignocellulose is, however, limited by its recalcitrant and heterogeneous structure which lowers accessibility to polysaccharides, such as cellulose, for industrial application. Elements which contribute to lignocellulose recalcitrance are so-called lignin–carbohydrate complexes (LCCs) [3]. LCCs are comprised of either ester, ether, or glycosidic covalent linkages, attaching lignin to plant polysaccharides. For example, cellulose microfibrils in grasses and wood are partially coated by xylan, which is linked through a glucuronic acid ester to lignin, thus tethering the lignin in proximity to the fibrils, and reducing cell wall accessibility to degradative enzymes [4,5]. The importance of this LCC linkage in cell wall assembly is indicated by the improved digestibility of plants lacking such linkages though the genetic manipulation to remove glucuronic acid substitution of xylan [6,7]. Glucuronoyl Esterases (GEs; EC 3.1.1.117) are, to date, the sole activity identified in Carbohydrate Esterase family 15 (CE15) in the carbohydrate-active enzymes database, CAZy [8]. GEs hydrolyse ester bonds between glucuronic acid residues of xylan and the alcohol moieties of lignin in LCCs [9,10]. All GEs identified so far are microbial. Fungal GEs (recently reviewed in [11]) were the first to be characterized [10], while in recent years many bacterial GEs (recently reviewed in [12]) from a variety of niches including marine species [13], plant symbionts [14] and rumen bacteria

* Corresponding author.
E-mail address: leila@chem.ku.dk (L. Lo Leggio).
[1] Current address: Department of Biotechnology and Biomedicine, Technical University of Denmark, Søltofts Plads, DK-2800 Kgs, Lyngby, Denmark.
[2] These authors contributed equally.

https://doi.org/10.1016/j.ijbiomac.2026.151020
Received 22 December 2025; Received in revised form 7 February 2026; Accepted 18 February 2026
Available online 19 February 2026

[15], have been identified. Since some CE15 members do not have clear GE activity *in vitro* [14,16,17] and their genes are found outside the expected genetic context (far from other genes involved in xylan degradation) [14,16] they may have very specialized saccharide preferences [16,18] and/or completely different functions [14].

The role of GEs in improving saccharification of lignocellulosic biomass has been demonstrated by involving selected CE15 enzymes in the hydrolysis of lignocellulosic material in combination with enzyme cocktails [9,15,19,20]. Therefore, since GEs are effective at improving the degradability of lignocellulosic plant material by enhancing accessibility of cellulose and hemicellulose, they are usually part of commercial lignocellulolytic enzyme cocktails where they are expected to act prior to or in concert with other depolymerizing enzymes in the initial stages of biomass hydrolysis [21].

Although great strides have been made in recent years to advance our understanding of GEs, still relatively little is known about their molecular interactions with larger substrates and products and about the nature of the biological substructures they target in the complex plant cell wall [22]. Many studies on GEs use small model substrates such as glucuronic acid esters [9], and only in rare cases comprise small lignin building blocks [23]. Unlike fungal CE15 enzymes, which have been suggested to require a 4-*O*-methyl substitution in the ligand to reach full activity [24], bacterial GEs can utilize nonmethylated glucuronic acid (GlcA) - and sometimes even galacturonic acid (GalA) - esters as substrates [9,18]. Activity on complex substrates obtained from natural biomass, for example a lignin-rich pellet, has also been clearly shown for selected GEs [25,26], but these studies are quite cumbersome, requiring LC-MS for analysis, and are rarely realistic on a routine basis. Some recent studies have employed a commercial coupled chromogenic assay based on the decorated xylobiose derivative $XU^{(4m)2}$-*p*-nitrophenol methyl ester (compact xylooligosaccharide nomenclature as in [27]) developed by Megazyme, which unfortunately has since been discontinued [17]. Even more recently, Koh et al. chemoenzymatically synthesized an $U^{4m2}XX$ benzyl ester and demonstrated much improved kinetic parameters compared to Bnz-GlcA for a fungal GE in an HPLC-based assay [28] and likewise higher binding affinity was measured for an inactive mutant of a different fungal GE and $U^{m4}XX^{-OH}$ compared to 4-*O*-methyl-Glc*p*A (4*O*MeGlcA) [29]. The latter studies in particular underscore the contribution of the saccharide backbone chain for interactions. Unfortunately, due to the difficulty in obtaining more realistic substrates containing the polysaccharide main chain, most kinetic studies still have to rely on the simple model substrates, where they may miss the effects of the interactions with the polysaccharide.

In terms of structural studies of GEs, the enzyme CE15A from the soil bacterium *Opitutus terrae* (*Ot*CE15A) has been an excellent model for structural studies of the interaction of bacterial GEs with complex oligosaccharides, and has also been extensively characterized with small model substrates [9,22] where it shows a very broad specificity. As a member of CE15, *Ot*CE15A is a α/β-hydrolase (ABH) with an α/β-sheet core made of eight β-strands connected by six α-helices [9,22]. *Ot*CE15A is a serine-type hydrolase with a catalytic triad located in a solvent-exposed cleft and composed by the catalytic Ser-267, His-408 and, particular to *Ot*CE15A, two partly functionally redundant acidic residues, Glu-290 and Asp-356 with the latter residue found at a noncanonical position [22,30], where most members of the family only have one [29,31]. A prominent role in both the acylation and deacylation steps of the reaction is played by Arg-268, whose side chain is proposed to form the oxyanion hole and to stabilize the tetrahedral intermediate [9,22,30]. Furthermore, the structures of *Ot*CE15A in complex with the product glucuronate, its covalent adducts, the glucuronoxylooligosaccharide β-D-Xyl*p*-(1→4)-[4-*O*-Me-α-D-Glc*p*A-(1→2)]-β-D-Xyl*p*-(1→4)-β-D-Xyl*p* (referred to as $XU^{4m2}X$) and xylobiose have been previously determined [22] and a number of variants characterized biochemically and structurally. This study centers on the hypothesis that GEs make extensive interactions with the polysaccharide in the LCC, and are thus true carbohydrate esterases – unlike other esterase families, which encompass structurally closely related members acting on both carbohydrate and non-carbohydrate containing substrates. We used crystallography as a tool to evaluate LCC fragments which could bind to *Ot*CE15A in a crystalline state. This approach can give a rough estimation of relative affinities of substructures with very low affinity and with only tiny amounts of compounds, which do not even need to be completely pure. As a result, the structure of *Ot*CE15A was obtained in complex with the heptasaccharide $XA^3XU^{4m2}X$ (Table 1), a β-1,4-linked xylopentaose with 4*O*MeGlcA and arabinofuranose (Ara*f*) decorations, the longest cell wall fragment bound to date in a GE crystal structure. The determination of the complex confirmed the interaction mode of *Ot*CE15A with $XU^{(4m)2}X$ revealing that the enzyme recognizes, or at least is able to bind, longer and decorated xylans. Comparing to other structurally characterized members in the family, it seems clear that not all will be able to adopt the same or similar binding mode(s). This result advances our understanding on the interaction mode of *Ot*CE15A with natural biomass polysaccharides and it provides useful insights on the activity of this enzyme in nature.

2. Materials and methods

2.1. Production of *Ot*CE15A

*Ot*CE15A was recombinantly produced in *Escherichia coli* BL21 (λDE3). Purification was performed as described previously [9] using immobilized metal ion affinity chromatography on an ÄKTA system (GE healthcare) using 5 mL HisTrap™ Excel columns, with 50 mM Tris-HCl (pH 8), 250 mM NaCl as binding buffer, and elution (binding buffer including 250 mM imidazole), followed by dialysis into 50 mM Tris-HCl buffer (pH 8). *Ot*CE15A was stored in buffer (50 mM Tris-HCl, pH 8, 100 mM NaCl) at 4 °C.

2.2. Commercial oligosaccharides and lignin analogues used for soaking

*Ot*CE15A's interaction with different ligands was investigated by soaking in preformed crystals of *Ot*CE15A. The chemical structures of the soaked compounds are reported in Table 1. Soaking with solutions of 2^3-L-arabinofuranosyl-xylotriose (A^2XX) and wheat arabinoxylan pentasaccharide (AXXX, where the side chain of arabinose is α-1,2 or α-1,3 linked) was performed (oligosaccharides were purchased from Megazyme). Other tested compounds were the lignin analogues guaiacol and 1,2-dimethoxybenzene (veratrole) in liquid form and 2,6-dimethoxyphenol and 1,2,3-trimethoxybenzene in solid form (all purchased from Sigma-Aldrich).

2.3. Separation of pine oligosaccharides

To obtain glucuronoxylooligosaccharides, Alcohol Insoluble Residue (AIR) from pine wood was prepared as previously described [32]. 0.55 g of AIR was treated with 4 M NaOH at room temperature (RT) for 1 h and centrifuged at 1180 *g* for 10 min. In order to remove the alkali, the supernatants were passed through a PD-10 column (Cytiva) and eluted with 50 mM ammonium acetate (pH 6.0) according to the manufacturer instructions to get the soluble hemicellulose. The eluate hemicellulose was used for xylanase XynC from *Bacteroides ovatus* (*Bo*XynC) digestion at 25 °C for 30 mins [33]. The *Bo*XynC xylanase was de-activated at 100 °C for 10 min and the hemicellulose was further digested with an excess of Xyn11A from *Neocallimastix patriciarum* (*Np*Xyn11A, from Megazyme, Bray, Ireland) in 50 mM ammonium acetate (pH 6.0) at 37 °C overnight and then lyophilized. Dried samples were re-suspended in 2 mL dH_2O, loaded onto a gravity driven preparative Bio-Gel P2 column (190 × 2.5 cm; BioRad), equilibrated, and run in 50 mM ammonium acetate (pH 6.0). Fractions were collected and dried *in vacuo*. Fractions of interest were monitored by polysaccharide analysis by carbohydrate electrophoresis (PACE) as described before [34] (Fig. 1A). To confirm the structure, fraction 26 and 30 were analysed by

Table 1
Chemical structure of the soaking compound and crystallization/soaking conditions for the soaked crystals. Crystallization conditions from Morpheus screen (Molecular Dimensions) as described in the experimental procedures.

Compound	Abbreviated chemical formula	Chemical structure	Crystallization condition (Morpheus screen)	Soaking condition	Result
α-L-Ara*f*-(1→2)-β-D-Xyl*p*-(1→4)-β-D-Xyl*p*-(1→4)-β-D-Xyl*p*	A^2XX	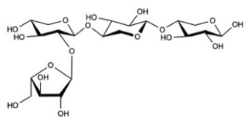	0.1 M alcohols, 1 M buffer system 1, pH 6.5, 37.5% v/v, precipitant mix 4.	5–500 mM in crystallization buffer, several minutes.	Datasets and structure obtained, but no bound ligand.
Wheat arabinoxylan pentasaccharide		Several structures (arabinose decorated β-1,4-linked xylooligosaccharides), e.g. 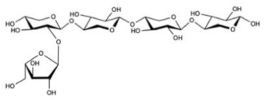	0.1 M ethylene glycols, 1 M buffer system 1, pH 6.5, 37.5% v/v, precipitant mix 4.	5 mM in crystallization buffer, several minutes.	Datasets and structure obtained, but no bound ligand.
o-Methoxyphenol (guaiacol)		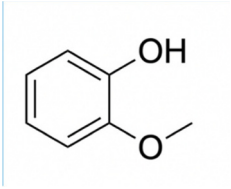	0.1 M amino acids, 0.1 M buffer system 1, pH 6.5, 30.00% v/v, precipitant mix 1.	Crystals transferred to solution of 900 mM guaiacol in crystallization buffer, soaking time up to 15 min.	Datasets and structure obtained, but no bound ligand.
1,2-Dimethoxybenzene (veratrole)		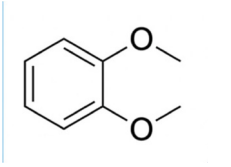	0.12 M alcohols, 0.1 M buffer system 1, pH 6.5, 30.00% v/v, precipitant mix 1.	Crystals transferred to solution of 700 mM 1,2 dimethoxybenzene-veratrole in crystallization buffer, soaking time up to 12 min.	Datasets and structure obtained, but no bound ligand.
2,6-Dimethoxyphenol		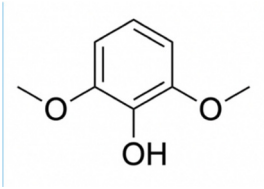	0.12 M alcohols, 0.1 M buffer system 1, pH 6.5, 30.00% v/v, precipitant mix 1.	1–2 crystals of the solid compound were minced, dissolved in mother liquor and added to the drop. Soaking time up to 17 min.	Datasets collected, but structures could not be refined.
1,2,3-Trimethoxybenzene		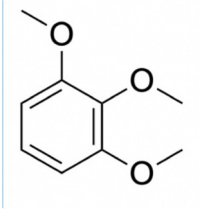	0.09 M halogens, 0.1 M buffer system 1, pH 6.5, 37.5% v/v, precipitant mix 4.	Solid added directly to the drop. Soaking time up to 4 min.	Compound poorly soluble, crystals damaged in soaking.
2^2-(4-*O*-Methyl-D-glucuronyl)-4^3-arabinofuranosyl-xylopentaose	$XA^3XU^{4m2}X$	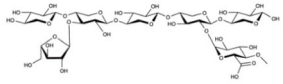	0.10 M carboxylic acids, 0.1 M buffer system 1, pH 6.5, 37.5% v/v, precipitant mix 4.	Solid added directly to the drop and crystals soaked for 2.5–20 min.	Structure determined for 15 min soak, see Table 2 and Results and discussion section.

MALDI-TOF-MS [35] (Fig. 1B).

2.4. Crystallization and ligand soaking

For crystallization, the previously described protocol was followed [22]. Crystals of *Ot*CE15A were prepared by sitting drop (0.3 μL drops) in MRC two-drop crystallization plates (Molecular Dimensions). Protein (7.2–9.5 mg/mL) was mixed with reservoir solutions in either a 3:1 or 1:1 ratio by aid of an Oryx 8 robot (Douglas Instruments) at room temperature. Crystals utilized for soaking and further data collection were obtained directly from Morpheus crystal screens (Molecular Dimensions) which from previous work were known to give well diffracting crystals under many conditions [22]. To avoid binding with saccharides other than the ligand, Morpheus crystal conditions containing monosaccharides as additives were avoided. Crystallization conditions used for soaked crystals as well as soaking conditions are given in Table 1. After soaking crystals were immediately picked in a cryoloop and flash frozen by plunging in liquid nitrogen.

2.5. Structure determination and refinement

Datasets used for structure determination were collected at the beamlines indicated in Table 2, while additional tests and data collections were carried out at BioMAX, MAX IV. A structure for a native

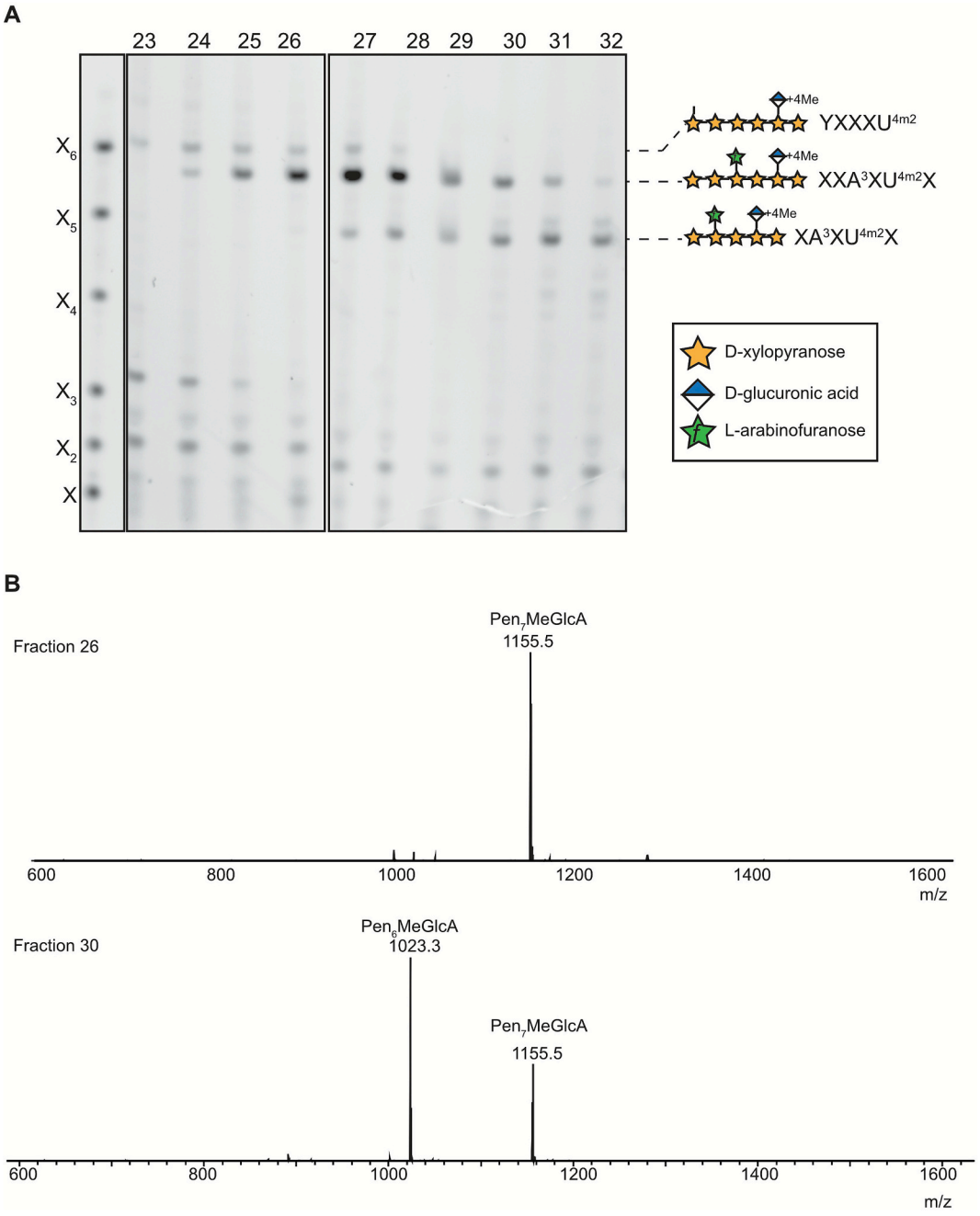

Fig. 1. Purification of GAX oligosaccharides. A: Pine wood was sequentially digested with *Bo*XynC and *Np*Xyn11A. The produced oligosaccharides were subsequently separated by bio-gel P2 column. Numbers 23 to 32 are fractions from the column. X–X6 are xylan standards. B: MS results of fraction 26 and 30.

crystal dataset isomorphous to the $XA^3XU^{4m2}X$ complex dataset (in $P2_12_12_1$ as opposed to P1, the more commonly observed space group for *Ot*CE15A crystals) was first determined by Molecular Replacement using as model structure *Ot*CE15A (PDB: 6GS0). The data were processed with the autoProc pipeline [36], including anisotropic correction with STARANISO [37]. Cycles of manual and computational refinement in Coot [38] and REFMAC5 [39] achieved an R_{factor} of 0.154 and R_{free} of 0.169. This structure was then used for solving the product complex by difference Fourier Methods. Data were automatically processed by the *XDSapp* pipeline [40] and manually rescaled with *XSCALE* [41] and *XDSCONV* [42] to adjust the resolution cut-off. The structure was refined in REFMAC5 [39] and Coot [38] in iterative cycles of manual and computational refinement until an R_{factor} of 0.168 and an R_{free} of 0.245 was achieved. The relatively large difference between the R_{factor} and R_{free} could not be minimized further and is attributed to the limited resolution of the diffraction data (2.40 Å compared to the uncomplexed data set extending beyond 1.4 Å). Refinement was continued while the R_{free} kept being reduced. Initial fitting of $XA^3XU^{4m2}X$ was made using the *Ot*CE15A structure in complex with $XU^{4m2}X$ (PDB: 6T0I) as a guide. The data collection, processing, and refinement statistics can be found in Table 2. The structures were independently validated using MOLProbity [43] and the wwPDB validation service [44]. The coordination geometry of the sodium ion present in both structures was further assessed using CheckMyMetal [45]. Identified outliers from these validation procedures were corrected, when feasible, prior to deposition in the PDB. PDB deposition ID's can be found in Table 2. Interactions between *Ot*CE15A and $XA^3XU^{4m2}X$ were analysed with Ligplot *via* a PDBsum analysis [46]. Solvent accessible surface area (ASA) and buried surface area (BSA) of the binding interface were additionally calculated with dr_sasa mode 1, Schüller lab [47]. This program calculates the ASA of

Table 2
Crystallographic statistics for *Ot*CE15A-Wt and *Ot*CE15A-Wt-$XA^3XU^{4m2}X$ in $P2_12_12_1$.

	*Ot*CE15A-Wt-$XA^3XU^{4m2}X$	*Ot*CE15A-Wt
Data collection		
Date	3rd September 2022	23rd September 2022
Source	P11 beamline at DESY	ID30B beamline at ESRF
Wavelength (Å)	1.03285	0.88560
Space group	$P2_12_12_1$	$P2_12_12_1$
Cell dimensions		
a, *b*, *c* (Å)	50.77, 65.43, 118.62	50.4, 64.5, 117.1
α, *β*, *γ* (°)	90, 90, 90	90, 90, 90
No. of measured reflections	67,450 (3226)	521,977 (8995)
No. of unique reflections	14,772 (898)	63,897 (3195)
Resolution (Å)	38.60–2.40 (2.47–2.40)	58.6–1.39 (1.49–1.39)
Ellipsoidal resolution limit (Å)	-	1.392 a*
	-	1.484 b*
	-	1.454 c*
R-meas (%)	18.4 (71.8)	8.6 (77.8)
$CC_{1/2}$ (%)	99.3 (78.6)	99.8 (57.7)
Mean I/σ	11.15 (2.42)	14.0 (1.6)
Completeness spherical (%)	92.3 (78.0) (all shells up to 2.99 Å have completeness >95%)	82.8 (23.6) (all shells up to 1.6 Å resolution have a spherical completeness >95%)
Completeness ellipsoidal (%)	–	91.1 (43.9)
Redundancy	4.5 (3.6)	8.2 (2.8)
Refinement		
R_{work}/R_{free}	0.168/0.245	0.154/0.169
No. of protein, ligand, ion, and water atoms	3104, 68, 1, 119	3160, 6, 11, 239
Average B-factors for protein, ligand, ion, and water (Å^2)	36.543, 71.683, 36.650, 33.697	16.405, 14.332, 34.838, 23.116
Bond length (Å) and angles (°) RMSD	0.0048, 1.3432	0.0109, 1.9000
Ramachandran favored, allowed and outliers (%)	98, 2, 0	96, 4, 0
PDB accession	9HUC	9HVR

the protein and ligand both in their unbound and bound states, using van der Waals radii compatible with NACCESS. The buried surface area (BSA) is then determined as the difference between the total ASA of the unbound molecules and their ASA in the complex, representing the surface area that becomes inaccessible upon binding—*i.e.*, the interface between the protein and ligand [47]. For each glycosidic bond connecting each subsite, the corresponding BSA of the oxygen atom was divided between the subsites. Lastly, all structures were visualized in PyMol [48] unless otherwise stated.

3. Results and discussion

3.1. Oligosaccharide content of the pine cell wall extract

It has been reported that the pine primary cell wall xylan is decorated with β(1→2)-Xyl*p* and α(1→2)-4*O*MeGlcA [49]. In pine secondary cell wall, xylan is modified by α(1→3)-Ara*f* and α(1→2)-4*O*MeGlcA [49,50]. Interestingly, the Ara*f* substitutions are located two xylose residues from 4*O*MeGlcA [50]. To test if the Ara*f* substitutions would impair the ability of *Ot*CE15A to bind oligosaccharides, we purified the glucuronoarabinoxylan (GAX) oligosaccharides from pine by size-exclusion chromatography. Fractions were monitored by PACE and MS which aided in identification of the oligosaccharide structures (Fig. 1). Fractions 23 to 26 were pooled and named as GAX1. In GAX1, there is one oligosaccharide with $YXXXU^{4m2}X$ structure from primary cell wall rich tissues (Y is backbone X substituted by the β(1→2)-Xyl*p* and one main oligosaccharide with $XXA^3XU^{(4m)2}X$ structure from secondary cell wall rich tissues (Fig. 1A). Both these two oligosaccharides were confirmed to have seven pentoses and one 4*O*MeGlcA (Fig. 1B) [49,50]. Fractions 27 to 31 were pooled and named as GAX2. In GAX2, there are also two oligosaccharides, $XXA^3XU^{4m2}X$ and $XA^3XU^{4m2}X$, which were found in similar proportions.

In order to choose suitable fractions for the soaking experiments, the *Ot*CE15A structure previously determined in complex with $XU^{4m2}X$ (PDB: 6T0I) was checked in proximity of the active site to verify that crystal packing allowed sufficient space. The analysis revealed that the enzyme can host an oligosaccharide longer than $XU^{4m2}X$ at the non-reducing end while the reducing end is blocked. Since all oligosaccharides in GAX1 and GAX2 only have one additional reducing end xylose after the uronic acid decoration, and thus should be able to fit, we examined the space extending from the non-reducing end and found it unlikely that longer oligosaccharides than $XA^3XU^{4m2}X$ could fit within the crystal. Thus, for the ligand soaking experiments, fraction GAX2, which contained a large proportion of $XA^3XU^{4m2}X$, was selected.

3.2. Crystallographic analysis to study interactions with substructures of the plant cell wall

The suggested biological role of *Ot*CE15A is to hydrolyse ester bonds which connect glucuronoxylan and lignin in plant cell walls, thereby reducing its recalcitrance. However, information on how GEs interact with their native substrates is still lacking, primarily due to difficulties with substrate acquisition and suitable detection methods [31]. Particularly, obtaining sufficient amounts of pure substructures of the plant cell wall to investigate with biophysical methods is highly challenging. Consequently, previous studies have primarily relied on monosaccharide-based model substrates, most commonly GlcA esters, which provide limited insight into the contributions of the xylan backbone and the lignin-derived ester moiety [9,30]. Here we used an alternative strategy to study the interactions with fragments of the plant cell wall using tiny amounts of partly purified material as well as chemical fragments that can be considered analogues of lignin. Of the tested compounds, only the pine cell wall digest gave clear indication of binding. Neither arabinooligosaccharides nor aromatic analogues of the lignin portion gave indication of binding, though structures after soaking could be obtained for most compounds (see overview in Table 1). The *Ot*CE15A structure was significantly affected when it was soaked with 2,6-dimethoxyphenol and from the comparison with previous experiments we could not predict if protein rearrangements were due to crystallization condition or to the soaking itself; however, structures could not be fully refined. When soaking with 1,2,3-trimethoxybenzene was performed, the compound did not dissolve well in mother liquor and it was directly added to the well, which negatively affected crystal quality, leading to data which could not be further analysed. However, aside from the compounds damaging the crystals, we can conclude that compounds devoid of the uronic acid moiety, such as small arabinoxylooligosaccharides devoid of glucuronate and some of the aromatic compounds do not bind even at high concentration and must therefore have very low affinity for *Ot*CE15A on their own. Lack of specific high affinity interaction with aromatic lignin-like compounds is perhaps to be expected given that unlike other GEs, *Ot*CE15A does not have a strong preference for specific ester substituents on GlcA substrates [9], and that computational analysis identified deacylation as the rate-limiting step [30]. In contrast, another GE, *Tt*CE15A, has been shown to be inhibited by aromatic containing acids (ferulic acid, sinapic acid and *p*-coumaric acid) which could also be considered lignin blocks mimics. Unfortunately *Tt*CE15A is less amenable to crystallographic studies due to the crystal form, lower resolution and less reproducible crystallization [31].

3.3. Structure of OtCE15A in complex with $XA^3XU^{4m2}X$

To investigate *Ot*CE15A specificity and mode of interaction with its

natural substrate, we performed soaking experiments with the glucuronoxylan $XA^3XU^{4m2}X$ enriched fraction obtained by hydrolytic activity of glycoside hydrolases on pine cell wall. When *Ot*CE15A was soaked for 15 min with the compound, a clear difference in electron density corresponding to a large oligosaccharide was observed bound near the known active site. We were thus able to determine the structure of the enzyme in complex with the polysaccharide fragment, the largest ligand in a CE15 protein structure to date (Fig. 2). We chose to model fully $XA^3XU^{4m2}X$, though the extreme xylose residues and the arabinose decoration are more poorly resolved, but lead to clear positive difference

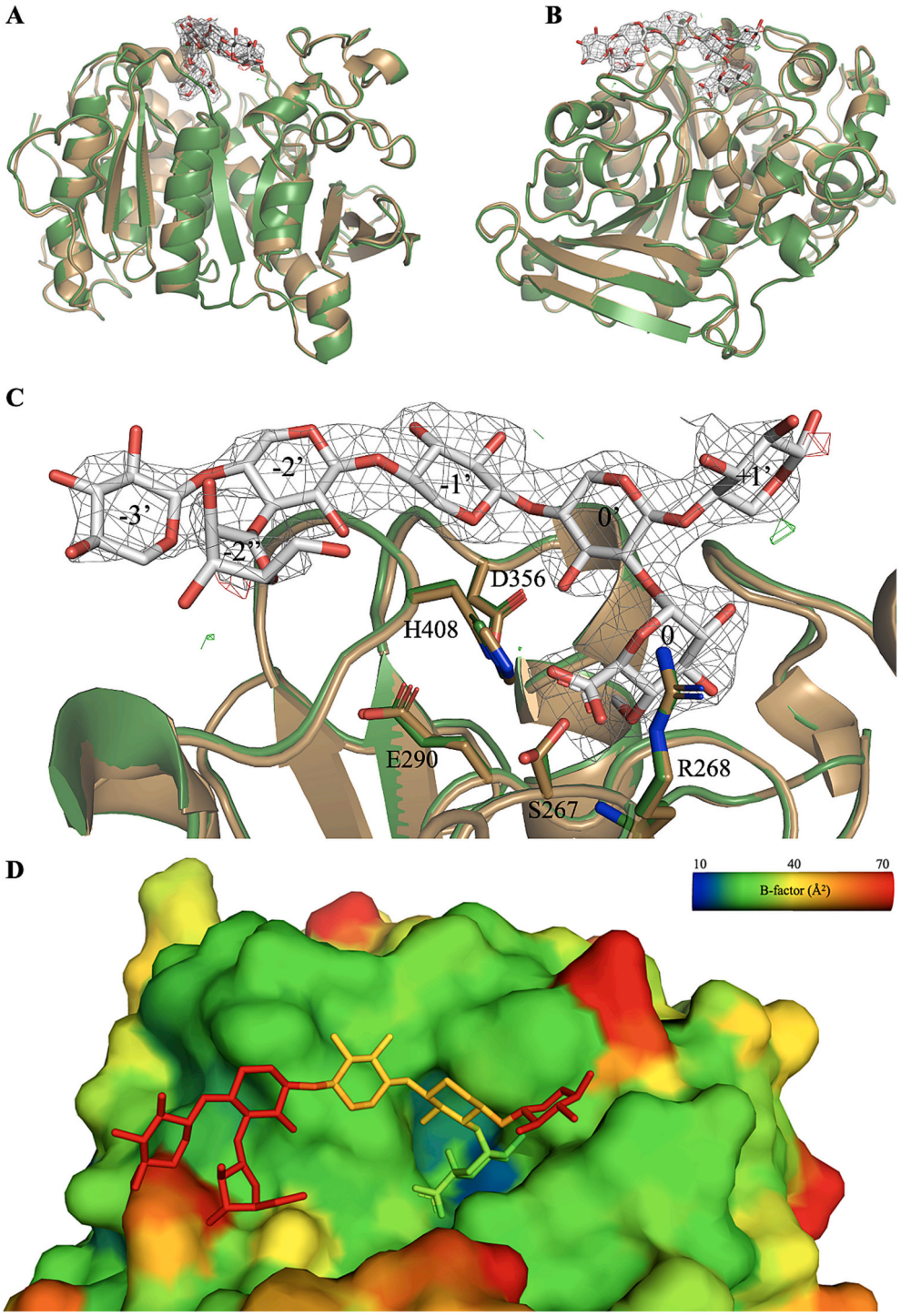

Fig. 2. Overview of *Ot*CE15A in complex with $XA^3XU^{4m2}X$. A: *Ot*CE15A (green) (PDB: 9HUC) is shown in cartoon with its ligand, $XA^3XU^{4m2}X$, represented in sticks. The electron density around the ligand is visualized with the 2Fo-Fc map (at 1.0 σ, grey mesh) and the Fo-Fc map (at 3.0 σ, negative: red and positive: green mesh). 9HUC is superimposed (with the PyMol align-command) with the native *Ot*CE15A in the same space group (bronze) (PDB: 9HVR) (full-atom RMSD: 0.602 Å and Cα RMSD: 0.340 Å). B: is turned 90° around the y-axis relative to A. C: $XA^3XU^{4m2}X$ shown with the active site residues and Arg268 (sticks). Subsites are numbered in analogy to previous glycoside hydrolase and esterase nomenclatures [51,52], with ' indicating subsites occupied by the main xylan chain which in this case can be considered a branch of the cleaved ester bond at subsite 0 (occupied by the uronic acid). The '' indicates the subsite occupied by the arabinose branch on the main xylan chain. D: The surface of *Ot*CE15A and $XA^3XU^{4m2}X$ is coloured according to B-factors (blue to red scale from low to high B-factors). All figures were produced with PyMol.

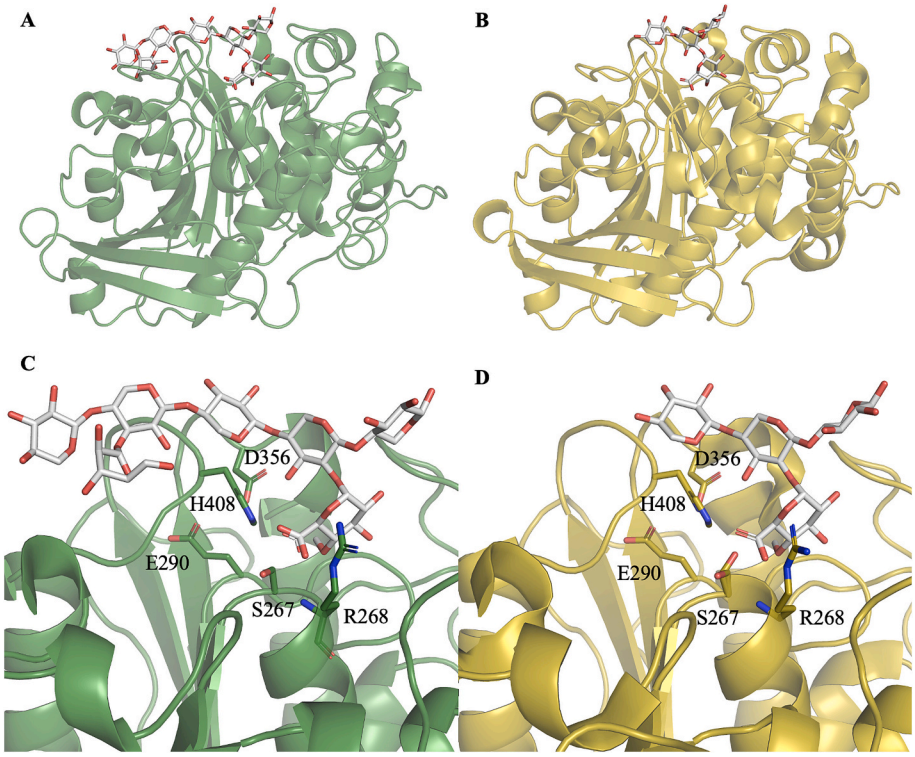

Fig. 3. Superimposed protein backbones of *Ot*CE15A-Wt-XA^{3}XU^{4m2}X (green, PDB: 9HUC) and *Ot*CE15A-Wt-XU^{4m2}X (yellow, PDB: 6T0I) shown side by side (overviews in A and B. respectively; zoomed view of the binding site in C and D, respectively) Image was created in PyMol using the align-command to superimpose the structures (full-atom RMSD: 1.133 Å and Cα RMSD: 0.996 Å) followed by the grid-command to visualize them separately.

density when they are omitted. The poorer electron density for these units is likely due to flexibility of the saccharides leading to different conformations in the crystal, also highlighted by higher B-factors.

Binding to this large ligand does not cause any major backbone conformational changes, as illustrated by the superposition of the *Ot*CE15A-Wt and *Ot*CE15A-Wt-XA^{3}XU^{4m2}X structures in $P2_12_12_1$ determined here (Fig. 3).

Structure determination revealed that *Ot*CE15A hosts the polysaccharide in the active site cleft and it mostly interacts with 4*O*MeGlcA moiety through H-bonds (2.5–3.2 Å; Fig. 4). The main residues involved are the Arginine that forms the oxyanion hole (R268) and the catalytic Serine (S267) and Histidine (H408) which all interact with the carboxyl group of GlcA. The arginine position and its interaction with the ligand confirms the significant contribution of this residue to position the substrate carboxyl group and to aid catalysis by stabilizing the oxyanion intermediate [22,30].

3.4. Detailed analysis of the interactions between OtCE15A and XA^{3}XU^{4m2}X

Detailed interactions are visualized in Fig. 4. As previously observed with smaller bound ligands [22], most of the hydrogen bonds between the ligand and *Ot*CE15A are formed through the 4*O*MeGlcA residue of the ligand at what, in analogy to previous nomenclatures for glycoside hydrolases and carbohydrate esterases [51,52], we have named subsite 0 (see Fig. 2 legend). Specifically, His408, Arg268, Lys271, Glu305, and Trp358 were identified to form hydrogen bonds with the 4*O*MeGlcA residue. Additional residues, both hydrophobic and hydrophilic (see below), interact with XA^{3}XU^{4m2}X with a single additional hydrogen bond interaction between subsite −2′ and the backbone of the catalytic histidine (His408).

A dr_sasa analysis of *Ot*CE15A with XA^{3}XU^{4m2}X was employed to assess the ASA and the BSA *i.e.*, the surface area of the protein and ligand that interacts with the solvent, and the area which is inaccessible to the solvent due to the protein-ligand interface, respectively. The analysis revealed that 239 Å^2 (90.9%) of the 4*O*MeGlcA surface area is buried within the protein structure, contributing to a total protein and ligand BSA of 356 Å^2 (Fig. 5A), which is slightly higher compared to the previously published *Ot*CE15A structure complexed with XU^{4m2}X with a total protein and ligand BSA of 325 Å^2 (Fig. 5B) [22] indicating a slightly larger intermolecular interface between 4*O*MeGlcA and subsite 0′ (Fig. 5B). These observations suggest that the extended non-reducing end of XA^{3}XU^{4m2}X affects how 4*O*MeGlcA interacts with *Ot*CE15A, slightly altering both the conformation and extent of the binding interface. As expected, the remaining 9.1% ASA of the 4*O*MeGlcA corresponds primarily to the O6A atom of the carboxylic acid group, which in the native substrate would form an ester linkage to the lignin moiety. In contrast, all other carbohydrate moieties of XA^{3}XU^{4m2}X exhibit BSAs below 50%, indicating that only one face of the saccharide forms an interface with the protein surface.

The BSAs per sugar moiety ranges from 38 Å^2 (at 0′ and − 3′) to 65 Å^2 (at −2″) and 72 Å^2 (at +1′) with an average for xyloses of 46.1 Å^2 while the total BSA (sugar + protein) at xylose binding subsites is 97.5 Å^2 (Fig. 5A). For comparison, we show interactions of several xylanases with unbranched and branched xylooligosaccharides (Fig. 5C–E) [53–55], where xylose residues each bury 37–199 Å^2 (avg. 116 Å^2) on binding, with total BSAs including protein of 79–281 Å^2 (avg. 198 Å^2) indicating on average significantly stronger interactions at GH subsites. It is however interesting to note that *Ta*Xyn10 in Fig. 5D, has demonstrated higher activity on feruloyl-arabinose-decorated as opposed to undecorated xylotriose [53] and likewise for *Cb*Xyn10A biochemical analysis showed that at least six subsites contribute favourably to binding and activity [54], suggesting that subsites with moderate total BSAs of ~150 Å^2 still contribute to binding. Thus, some *Ot*CE15A subsites (−2″ and +1′), with comparable BSAs, are likely to also energetically contribute to binding, together with the uronic acid moiety.

The dr_sasa analysis also identified 16 residues that are in direct contact with 4*O*MeGlcA. Among these, Arg268, Ser267, Glu305, and

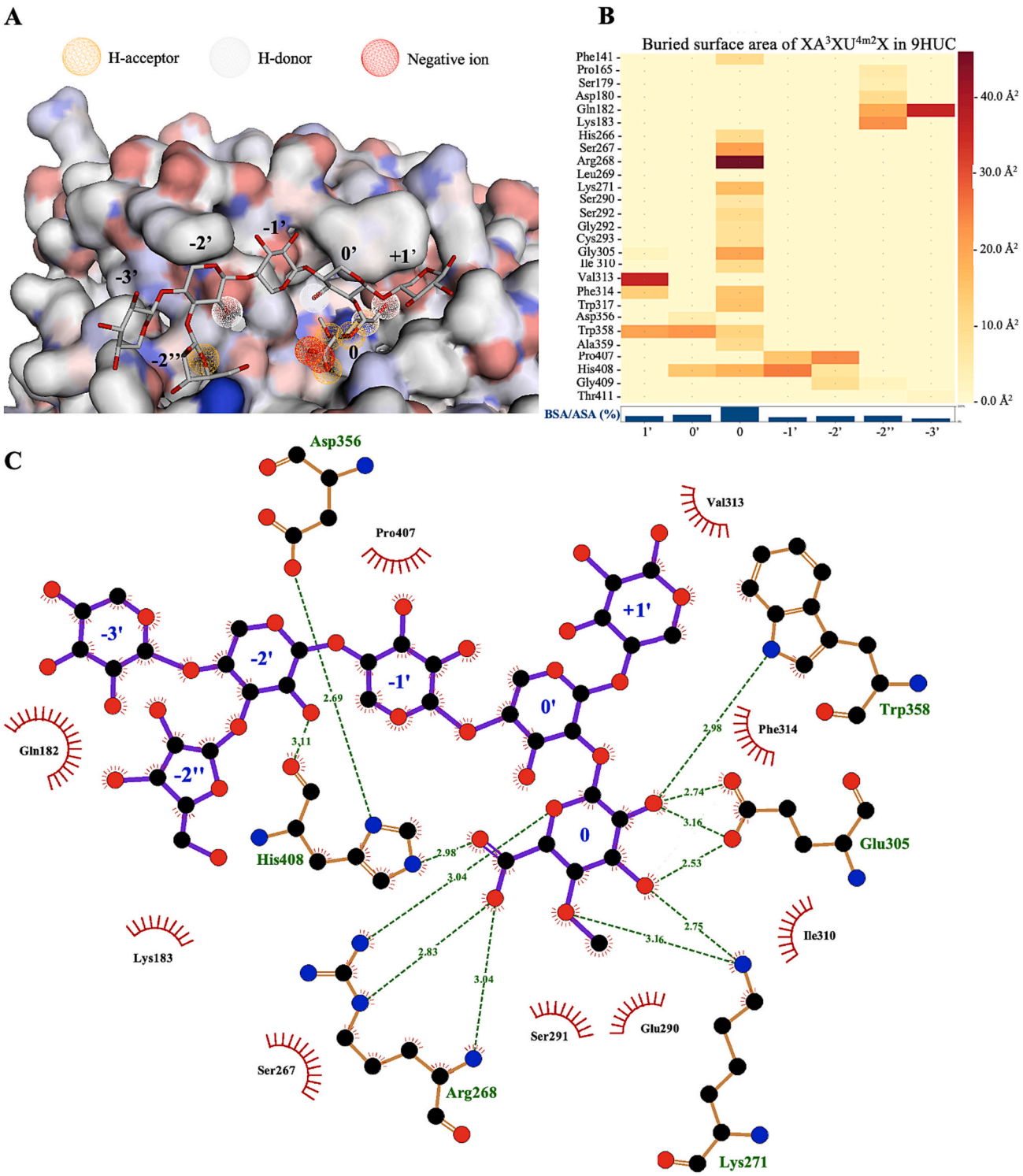

Fig. 4. Detailed interactions of *Ot*CE15A-Wt with $XA^3XU^{4m2}X$. A: Pharmit plot of *Ot*CE15A: $XA^3XU^{4m2}X$ interactions. Orange mesh indicates H-acceptor, white mesh indicate H-donors, and red mesh indicate negative charges [56]. B: dr_sasa heatmap of showing amino-acid residues interfacing the subsites of $XA^3XU^{4m2}X$. The bottom histogram shows the percentage of BSA ($Å^2$) for each subsite [47]. C: Ligplot diagram based on PDBsum analysis [46,57]. Dashed lines indicate hydrogen bonds, while dashed semicircles indicate other contacts.

His408 form the largest interfaces with 4*O*MeGlcA (Fig. 4B). The methyl group, which is often invoked as essential for fungal GE action, interacts primarily with Glu290, Ser291 and Ala359 (and additionally seven other residues). Notably, the xylose at subsite $+1'$ interacts with two hydrophobic residues, Val313 and Phe314. The other end of the xylan chain interfaces with hydrophilic residues, such as Gln182, which interacts with both sugar units at subsites $-2''$ and $-3'$ through hydroxyl groups and van der Waals interactions with the carbon ring. Additionally, $-2''$ forms notable interfaces with Lys183. These residues (180–183) are part of Reg2, a region often present (though not necessarily structurally conserved) in bacterial GEs but most often absent in fungal GEs [9].

Similarly to *Ot*CE15A in complex with $XU^{4m2}X$, the xylopentaose portion is less involved in polar interactions but the presence of aromatic

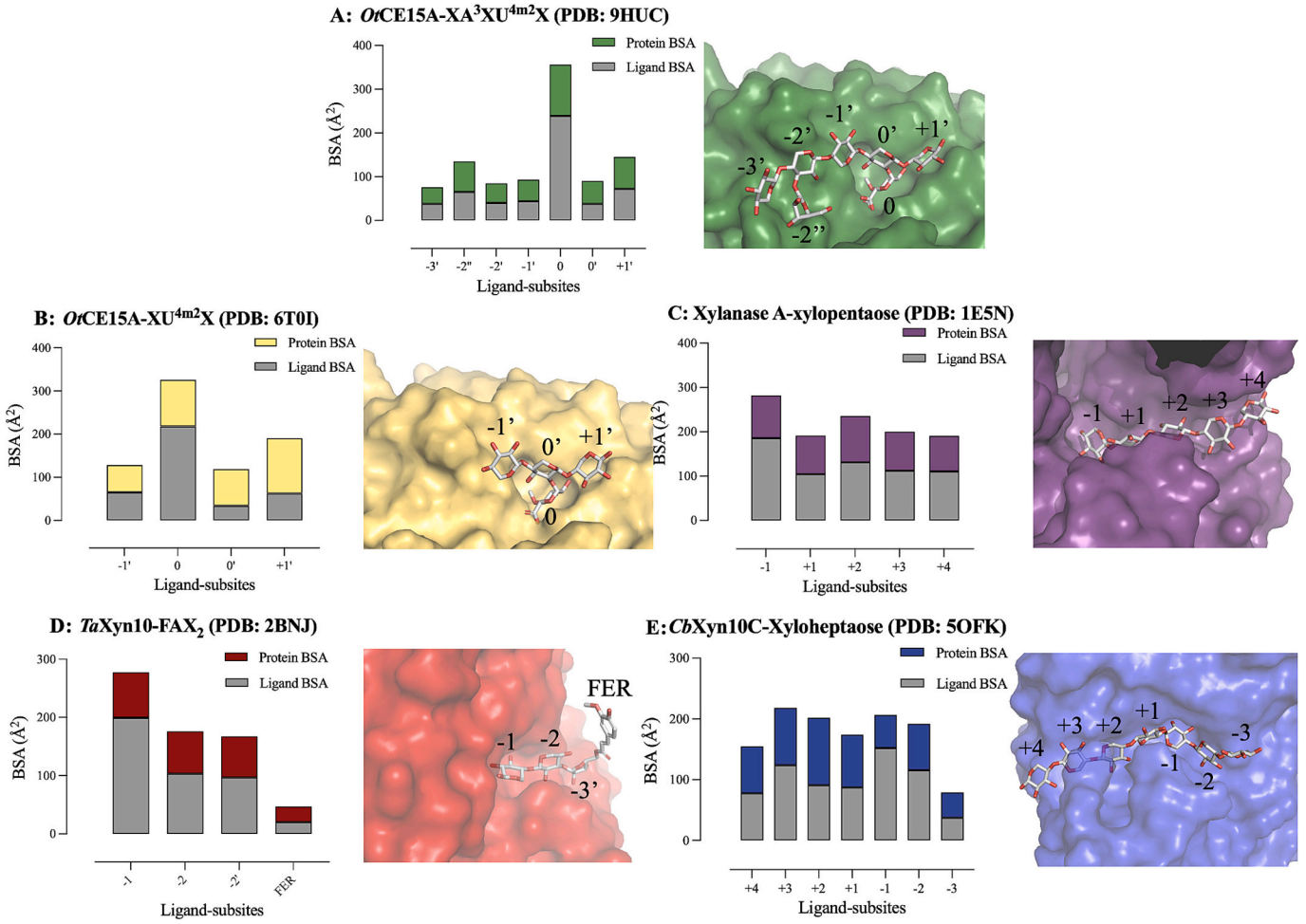

Fig. 5. Buried surface area analysis, between protein (coloured column) and ligand (grey column) subsites with dr_sasa mode 1 [47]. A: *Ot*CE15A-XA^{3}XU^{4m2}X (PDB: 9HUC). B: *Ot*CE15A-XU^{4m2}X (PDB: 6T0I) [22]. C: Xylanase A-xylopentaose (PDB: 1E5N) [55]. D: *Ta*Xyn10-FAX$_2$ (PDB: 2BNJ) [53]. E: *Cb*Xyn10C-Xyloheptaose (PDB: 5OFK) [54].

residues like Trp358, Phe314 and Trp317 allows π-π interaction with the carbohydrate substrate. Other aromatic residues (Phe141 and Tyr142) are also close to the expected 'lignin side' of the ester, which would project to contact the area marked in Fig. 6A (as previously suggested) [9]. The lack of hydrogen bonds between *Ot*CE15A and the xylan chain of the substrate perhaps could allow the enzyme to accommodate

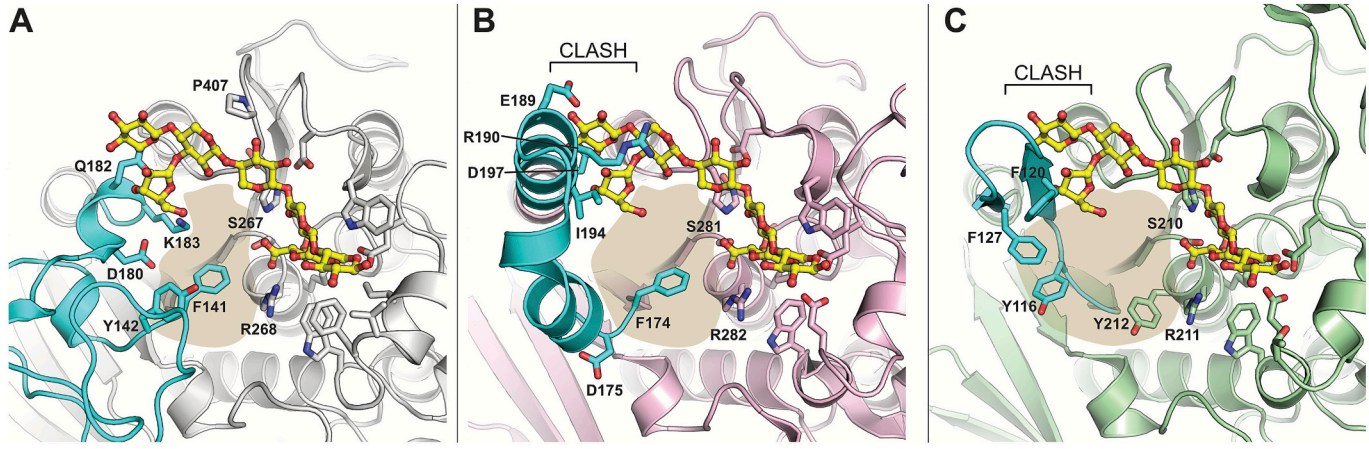

Fig. 6. Comparison of select bacterial GEs. The active site of (A) *Ot*CE15A in complex with XA^{3}XU^{4m2}X (PDB: 9HUC), (B) *Tt*CE15A (PDB: 6HSW) and (C) *Ck*CE15 (PDB: 7NN3) [31,58] both with the ligand in the same position generated by structural alignment with *Ot*CE15A in panel A. Reg2 in all proteins is coloured in cyan. Relevant residues found in Reg2, the catalytic serine, and oxyanion stabilizing arginine are labelled for each protein. The proposed position of the lignin binding is highlighted in light brown. Note the differences in Reg2 in *Tt*CE15A and *Ck*CE15 would lead to steric clashes with ligand in the same position observed in the complex with *Ot*CE15A.

diversely decorated xylan substrates as would be expected in interaction with LCCs [12]. As the structure of *Ot*CE15A in complex with $XU^{4m2}X$ suggested, also in this space group the reducing end of the polysaccharide backbone is partly blocked by a symmetry-related molecule, while the non-reducing end could extend further. However, the non-reducing end of the oligosaccharide gets farther from the main structure, interacting less with the enzyme, and therefore we cannot predict a strong interaction with longer polysaccharidic substrates. Nevertheless, a previously identified secondary surface binding site for xylobiose, involving H-bond interactions with the backbone of Ala223 and Ser218, may provide additional anchoring points for longer glucuronoxylan chains [22]. Such interactions could enable extended substrates to associate with the enzyme surface while accommodating decorations at multiple positions along the xylan backbone. It is however unknown at what specific stage of the biomass degradation GEs interact in a natural setting, and decorated oligosaccharides may indeed best represent the natural substrate. As noted before, aside from the highly conserved interactions with the uronic acid moiety, there is very little conservation of residues in the substrate binding surface among CE15 members. Furthermore, we observe that in other bacterial GEs [31,58] where the structure of Reg2 is different than in *Ot*CE15A, there would be considerable clashes between Reg2 and $XA^3XU^{4m2}X$ if bound identically as in the structure presented here (Fig. 6) suggesting there could be enzyme specificity for different carbohydrate portions of the polymeric substrate. However, Reg2 has been found to have higher B-factors than the rest of the protein in structures of bacterial CE15 enzymes [9,31,58], indicating that these regions are likely flexible and possibly dynamic, which could result in movements that accommodate larger or diversely decorated xylan substrates.

4. Conclusions

The plant cell wall, especially *in planta*, is a very heterogenous and complex structure, and ultimately, research on structure-function relationships is limited by the state-of-the-art in visualizing proteins *in situ* on intact plant biomass, at sufficient resolution to both determine binding moieties on the enzyme and on the lignin-carbohydrate complexes. Furthermore, since the details of temporal and spatial action of specific enzymes on specific tissues are rarely known, the exact structures attacked by the enzymes may be transient. Within this inherent limitation, soaking of native *Ot*CE15A with a plant-derived glucuronoxylooligosaccharide $XA^3XU^{4m2}X$ yielded here a complex with the largest carbohydrate bound to a CE15 enzyme to date, which has thereby permitted detailed studies of its protein-substrate interactions. This structure proves, among other things that decorations of the oligosaccharide-, and by proxy likely polysaccharide-derived substrates can be accommodated. The interactions suggest that the active site cleft hosts the carbohydrate chain but that the main contacts between the enzyme and the substrate are to the GlcA moiety and the arabinofuranosyl decoration. The almost complete lack of hydrogen bonds aside from the 4*O*MeGlcA residue, while maintaining a significant contact surface area compared to other poly- or oligosaccharide-degrading enzymes, suggests versatile binding which is compatible with the heterogeneity of LCCs. This versatility is also a great advantage for industrial applications when a variable and heterogeneous material like lignocellulosic waste biomass is involved. A major remaining challenge for this enzyme type is now to study the interaction with the lignin portion of the substrate, *e.g.* by advanced computational simulations taking experimental structural information as a starting point. Looking further into the future, recent developments in *e.g.* integration of tomographic and microscopy techniques hold the promise that at some stage direct multiscale visualization (including high resolution) of enzymes on complex matrices will be possible [59].

CRediT authorship contribution statement

A. Zaghini: Writing – original draft, Investigation. **E.B. Østberg:** Writing – original draft, Visualization, Validation, Investigation. **S. Banerjee:** Writing – review & editing, Supervision. **S. Mazurkewich:** Writing – review & editing, Visualization, Resources. **L. Yu:** Writing – original draft, Visualization, Resources, Investigation. **P. Dupree:** Writing – review & editing, Supervision, Resources. **J. Larsbrink:** Writing – review & editing, Project administration, Funding acquisition, Conceptualization. **L. Lo Leggio:** Writing – original draft, Supervision, Project administration, Funding acquisition, Conceptualization.

Funding

We thank the Novo Nordisk Foundation for funding under grant NNF21OC0071611.

Declaration of competing interest

All authors declare no conflict of interest in this research.

Acknowledgments

Crystallization with the Oryx 8 robot (Douglas Instruments) was set up by Mohannad Khaled Aloula. We thank Yusuf Theibich for general assistance with crystal soaking and Tanguy Scaillet for the crystal soaking of arabinose decorated xylooligosaccharide (pentasaccharide).

We thank the European Synchrotron Radiation Facility (ESRF) and for beamline access and under the proposal I-20220632 EC, and the Deutsches Elektronen-Synchrotron (DESY) for beamline access under the proposal. We thank Johanna Hakanpää for assistance at the DESY P11 beamline. Additional crystals were tested at the Biomax beamline at the MAX IV synchrotron, Lund, Sweden. Travels to synchrotrons were supported by the Danish Ministry of Higher Education and Science through the instrument center DANSCATT.

Data availability

Crystallographic data and structures are deposited with the Protein Data Bank (codes 9HUC and 9HVR)

References

[1] X. Zhao, L. Zhang, D. Liu, Biomass recalcitrance. Part I: the chemical compositions and physical structures affecting the enzymatic hydrolysis of lignocellulose, Biofuels Bioprod. Biorefin. 6 (2012) 465–482, https://doi.org/10.1002/BBB.1331.
[2] A.P. Ingle, S. Saxena, M.P. Moharil, J.D. Rivaldi, L. Ramos, A.K. Chandel, Production of biomaterials and biochemicals from lignocellulosic biomass through sustainable approaches: current scenario and future perspectives, Biotechnol. Sustain. Mater. 2 (2025) 3, https://doi.org/10.1186/s44316-025-00025-2.
[3] N. Giummarella, Y. Pu, A.J. Ragauskas, M. Lawoko, A critical review on the analysis of lignin carbohydrate bonds, Green Chem. 21 (2019) 1573–1595, https://doi.org/10.1039/c8gc03606c.
[4] T.J. Simmons, J.C. Mortimer, O.D. Bernardinelli, A.C. Pöppler, S.P. Brown, E.R. DeAzevedo, R. Dupree, P. Dupree, Folding of xylan onto cellulose fibrils in plant cell walls revealed by solid-state NMR, Nat. Commun. 2016 7:1 7 (2016) 13902-. doi:https://doi.org/10.1038/ncomms13902.
[5] O.M. Terrett, P. Dupree, Covalent interactions between lignin and hemicelluloses in plant secondary cell walls, Curr. Opin. Biotechnol. 56 (2019) 97–104, https://doi.org/10.1016/j.copbio.2018.10.010.
[6] R.H. Gallinari, J.J. Lyczakowski, J.P.P. Llerena, J.L.S. Mayer, S.C. Rabelo, M. Menossi Teixeira, P. Dupree, P. Araujo, Silencing ScGUX2 reduces xylan glucuronidation and improves biomass saccharification in sugarcane, Plant Biotechnol. J. 22 (2024) 587–601, https://doi.org/10.1111/pbi.14207.
[7] T. Tryfona, Y. Pankratova, D. Petrik, D. Rebaque Moran, R. Wightman, X. Yu, A. Echevarría-Poza, P.K. Deralia, F. Vilaplana, C.T. Anderson, M. Hong, P. Dupree, Altering the substitution and cross-linking of glucuronoarabinoxylans affects cell wall architecture in *Brachypodium distachyon*, New Phytol. 242 (2024) 524–543, https://doi.org/10.1111/nph.19624.
[8] E. Drula, M.L. Garron, S. Dogan, V. Lombard, B. Henrissat, N. Terrapon, The carbohydrate-active enzyme database: functions and literature, Nucleic Acids Res. 50 (2022) D571–D577, https://doi.org/10.1093/NAR/GKAB1045.

[9] J. Arnling Bååth, S. Mazurkewich, R.M. Knudsen, J.C.N. Poulsen, L. Olsson, L. Lo Leggio, J. Larsbrink, Biochemical and structural features of diverse bacterial glucuronoyl esterases facilitating recalcitrant biomass conversion, Biotechnol. Biofuels 11 (2018), https://doi.org/10.1186/s13068-018-1213-x.

[10] S. Špániková, P. Biely, Glucuronoyl esterase - novel carbohydrate esterase produced by *Schizophyllum commune*, FEBS Lett. 580 (2006) 4597–4601, https://doi.org/10.1016/j.febslet.2006.07.033.

[11] J.W. Agger, M.S. Madsen, L.K. Martinsen, P.A. Martins, K. Barrett, A.S. Meyer, New insights to diversity and enzyme–substrate interactions of fungal glucuronoyl esterases, Appl. Microbiol. Biotechnol. 107 (2023) 4447–4457, https://doi.org/10.1007/s00253-023-12575-4.

[12] J. Larsbrink, L. Lo Leggio, Glucuronoyl esterases – enzymes to decouple lignin and carbohydrates and enable better utilization of renewable plant biomass, Essays Biochem. 67 (2023) 493–503, https://doi.org/10.1042/EBC20220155.

[13] C. De Santi, O.A. Gani, R. Helland, A. Williamson, Structural insight into a CE15 esterase from the marine bacterial metagenome, Sci. Rep. 7 (2017), https://doi.org/10.1038/s41598-017-17677-4.

[14] M. Carbonaro, S. Mazurkewich, G. Fiorentino, L. Lo Leggio, J. Larsbrink, Exploration of three *Dyadobacter fermentans* enzymes uncovers molecular activity determinants in CE15, Appl. Microbiol. Biotechnol. 108 (2024), https://doi.org/10.1007/s00253-024-13175-6.

[15] R.J. Gruninger, M. Kevorkova, K.E. Low, D.R. Jones, L. Worrall, T.A. McAllister, D. W. Abbott, Structural, biochemical, and phylogenetic analysis of bacterial and fungal carbohydrate esterase family 15 glucuronoyl esterases in the rumen, Protein J. 43 (2024) 910–922, https://doi.org/10.1007/s10930-024-10221-0.

[16] S. Mazurkewich, K.C. Scholzen, R.H. Brusch, J.C.N. Poulsen, Y. Theibich, S. Hüttner, L. Olsson, J. Larsbrink, L. Lo Leggio, Structural and functional investigation of a fungal member of carbohydrate esterase family 15 with potential specificity for rare xylans, Acta Crystallogr. D Struct. Biol. 79 (2023) 545–555, https://doi.org/10.1107/S205979832300325X.

[17] M.S. Madsen, P.A. Martins, J.W. Agger, Efficient activity screening of new glucuronoyl esterases using a pNP-based assay, Enzym. Microb. Technol. 178 (2024), https://doi.org/10.1016/j.enzmictec.2024.110444.

[18] A. Seveso, S. Mazurkewich, S. Banerjee, J.C.N. Poulsen, L. Lo Leggio, J. Larsbrink, Polysaccharide utilization loci from Bacteroidota encode CE15 enzymes with possible roles in cleaving pectin-lignin bonds, Appl. Environ. Microbiol. 90 (2024), https://doi.org/10.1128/aem.01768-23.

[19] C. D'Errico, J. Börjesson, H. Ding, K.B.R.M. Krogh, N. Spodsberg, R. Madsen, R. N. Monrad, Improved biomass degradation using fungal glucuronoyl-esterases-hydrolysis of natural corn fiber substrate, J. Biotechnol. 219 (2016) 117–123, https://doi.org/10.1016/j.jbiotec.2015.12.024.

[20] C. D'Errico, J.O. Jørgensen, K.B.R.M. Krogh, N. Spodsberg, R. Madsen, R. N. Monrad, Enzymatic degradation of lignin-carbohydrate complexes (LCCs): model studies using a fungal glucuronoyl esterase from *Cerrena unicolor*, Biotechnol. Bioeng. 112 (2015) 914–922, https://doi.org/10.1002/bit.25508/abstract.

[21] O. Raji, J. Arnling Bååth, T. V. Vuong, J. Larsbrink, L. Olsson, E.R. Master, The coordinated action of glucuronoyl esterase and α-glucuronidase promotes the disassembly of lignin–carbohydrate complexes, FEBS Lett. 595 (2021) 351–359. doi:https://doi.org/10.1002/1873-3468.14019;JOURNAL:JOURNAL:18733468.

[22] S. Mazurkewich, J.C.N. Poulsen, L. Lo Leggio, J. Larsbrink, Structural and biochemical studies of the glucuronoyl esterase OtCE15A illuminate its interaction with lignocellulosic components, J. Biol. Chem. 294 (2019) 19978–19987, https://doi.org/10.1074/JBC.RA119.011435.

[23] C. Pentari, C. Katsimpouras, M. Haon, J.G. Berrin, A. Zerva, E. Topakas, Exploring the synergy between fungal CE15 glucuronoyl esterases and xylanases for lignocellulose saccharification, Biotechnol. Biofuels Bioprod. 18 (2025), https://doi.org/10.1186/S13068-025-02639-0.

[24] M. Ďuranová, J. Hirsch, K. Kolenová, P. Biely, Fungal glucuronoyl esterases and substrate uronic acid recognition, Biosci. Biotechnol. Biochem. 73 (2009) 2483–2487, https://doi.org/10.1271/bbb.90486.

[25] C. Mosbech, J. Holck, A.S. Meyer, J.W. Agger, The natural catalytic function of CuGE glucuronoyl esterase in hydrolysis of genuine lignin-carbohydrate complexes from birch, Biotechnol. Biofuels 11 (2018), https://doi.org/10.1186/s13068-018-1075-2.

[26] J. Arnling Bååth, N. Giummarella, S. Klaubauf, M. Lawoko, L. Olsson, A glucuronoyl esterase from *Acremonium alcalophilum* cleaves native lignin-carbohydrate ester bonds, FEBS Lett. 590 (2016) 2611–2618, https://doi.org/10.1002/1873-3468.12290.

[27] R. Fauré, C.M. Courtin, J.A. Delcour, C. Dumon, C.B. Faulds, G.B. Fincher, S. Fort, S.C. Fry, S. Halila, M.A. Kabel, L. Pouvreau, B. Quemener, A. Rivet, L. Saulnier, H. A. Schols, H. Driguez, M.J. O'Donohue, A brief and informationally rich naming system for oligosaccharide motifs of heteroxylans found in plant cell walls, Aust. J. Chem. 62 (2009) 533–537, https://doi.org/10.1071/CH08458.

[28] S. Koh, Y. Saito, H. Kudo, S. Taguchi, A. Kumagai, M. Mizuno, M. Samejima, Y. Amano, Synthesis of a natural core substrate with lignin-xylan cross-linkage for unveiling the productive kinetic parameters of glucuronoyl esterase, Biochem. Biophys. Res. Commun. (2024) 150642, https://doi.org/10.1016/j.bbrc.2024.150642.

[29] H.A. Ernst, C. Mosbech, A.E. Langkilde, P. Westh, A.S. Meyer, J.W. Agger, S. Larsen, The structural basis of fungal glucuronoyl esterase activity on natural substrates, Nat. Commun. 11 (2020), https://doi.org/10.1038/s41467-020-14833-9.

[30] Z. Zong, S. Mazurkewich, C.S. Pereira, H. Fu, W. Cai, X. Shao, M.S. Skaf, J. Larsbrink, L. Lo Leggio, Mechanism and biomass association of glucuronoyl esterase: an α/β hydrolase with potential in biomass conversion, Nat. Commun. 13 (2022), https://doi.org/10.1038/s41467-022-28938-w.

[31] J.A. Bååth, S. Mazurkewich, J.C.N. Poulsen, L. Olsson, L. Lo Leggio, J. Larsbrink, Structure-function analyses reveal that a glucuronoyl esterase from *Teredinibacter turnerae* interacts with carbohydrates and aromatic compounds, J. Biol. Chem. 294 (2019) 6635–6644, https://doi.org/10.1074/jbc.RA119.007831.

[32] F. Goubet, C.J. Barton, J.C. Mortimer, X. Yu, Z. Zhang, G.P. Miles, J. Richens, A. H. Liepman, K. Seffen, P. Dupree, Cell wall glucomannan in Arabidopsis is synthesised by CSLA glycosyltransferases, and influences the progression of embryogenesis, Plant J. 60 (2009) 527–538, https://doi.org/10.1111/j.1365-313X.2009.03977.x.

[33] L. Yu, L.F.L. Wilson, O.M. Terrett, J. Wurman-Rodrich, J.J. Łyczakowski, X. Yu, K. B.R.M. Krogh, P. Dupree, Evolution of glucuronoxylan side chain variability in vascular plants and the compensatory adaptations of cell wall–degrading hydrolases, New Phytol. (2024), https://doi.org/10.1111/nph.19957.

[34] L. Yu, Y. Yoshimi, R. Cresswell, R. Wightman, J.J. Lyczakowski, L.F.L. Wilson, K. Ishida, K. Stott, X. Yu, S. Charalambous, J. Wurman-Rodrich, O.M. Terrett, S. P. Brown, R. Dupree, H. Temple, K.B.R.M. Krogh, P. Dupree, Eudicot primary cell wall glucomannan is related in synthesis, structure, and function to xyloglucan, Plant Cell 34 (2022) 4600–4622, https://doi.org/10.1093/plcell/koac238.

[35] T. Tryfona, H.C. Liang, T. Kotake, Y. Tsumuraya, E. Stephens, P. Dupree, Structural characterization of Arabidopsis leaf arabinogalactan polysaccharides, Plant Physiol. 160 (2012) 653–666, https://doi.org/10.1104/pp.112.202309.

[36] C. Vonrhein, C. Flensburg, P. Keller, A. Sharff, O. Smart, W. Paciorek, T. Womack, G. Bricogne, Data processing and analysis with the autoPROC toolbox, Acta Crystallogr. D Biol. Crystallogr. 67 (2011) 293–302, https://doi.org/10.1107/S0907444911007773.

[37] I.J. Tickle, C. Flensburg, P. Keller, W. Paciorek, A. Sharff, C. Vonrhein, G. Bricogne, STARANISO, 2016.

[38] P. Emsley, B. Lohkamp, W.G. Scott, K. Cowtan, Features and development of *Coot*, Acta Crystallogr. D Biol. Crystallogr. 66 (2010) 486–501, https://doi.org/10.1107/S0907444910007493.

[39] S. McNicholas, E. Potterton, K.S. Wilson, M.E.M. Noble, Presenting your structures: the CCP4mg molecular-graphics software, Acta Crystallogr. D Biol. Crystallogr. 67 (2011) 386–394, https://doi.org/10.1107/S0907444911007281.

[40] W. Kabsch, XDS, Urn:Issn:0907-4449 66 (2010) 125–132. doi:https://doi.org/10.1107/S0907444909047337, Acta Crystallogr. Sect. D Biol. Crystallogr..

[41] W. Kabsch, Integration, scaling, space-group assignment and post-refinement, Acta Crystallogr. D Biol. Crystallogr. 66 (2010) 133–144, https://doi.org/10.1107/S0907444909047374.

[42] W. Furey, K.D. Cowtan, K.Y.J. Zhang, P. Main, A.T. Brunger, P.D. Adams, W.L. DeLano, P. Gros, R.W. Grosse-Kunstleve, J.-S. Jiang, N.S. Pannu, R.J. Read, L.M. Rice, T. Simonson, D.E. Tronrud, L.F. Ten Eyck, V.S. Lamzin, A. Perrakis, K.S. Wilson, R.A. Laskowski, M.W. MacArthur, J.M. Thornton, P.J. Kraulis, D.C. Richardson, J.S. Richardson, W. Kabsch, G.M. Sheldrick, XDSCONV, Urn:Isbn:978-0-7923-6857-1 F (2006) 695–743. doi:https://doi.org/10.1107/97809553602060000724.

[43] C.J. Williams, J.J. Headd, N.W. Moriarty, M.G. Prisant, L.L. Videau, L.N. Deis, V. Verma, D.A. Keedy, B.J. Hintze, V.B. Chen, S. Jain, S.M. Lewis, W.B. Arendall, J. Snoeyink, P.D. Adams, S.C. Lovell, J.S. Richardson, D.C. Richardson, MolProbity: more and better reference data for improved all-atom structure validation, Protein Sci. 27 (2018) 293–315, https://doi.org/10.1002/PRO.3330.

[44] wwPDB Validation Service, (2025). https://validate-rcsb-2.wwpdb.org/ (accessed December 11, 2024).

[45] M. Gucwa, J. Lenkiewicz, H. Zheng, M. Cymborowski, D.R. Cooper, K. Murzyn, W. Minor, CMM—an enhanced platform for interactive validation of metal binding sites, Protein Sci. 32 (2023) e4525, https://doi.org/10.1002/PRO.4525.

[46] R.A. Laskowski, M.B. Swindells, LigPlot+: multiple ligand-protein interaction diagrams for drug discovery, J. Chem. Inf. Model. 51 (2011) 2778–2786, https://doi.org/10.1021/CI200227U.

[47] J. Ribeiro, C. Ríos-Vera, F. Melo, A. Schüller, Calculation of accurate interatomic contact surface areas for the quantitative analysis of non-bonded molecular interactions, Bioinformatics 35 (2019) 3499–3501, https://doi.org/10.1093/bioinformatics/btz062.

[48] L. Schrödinger, The PyMOL Molecular Graphics System, Version 3.0, (n.d.).

[49] H. Temple, Y. Yoshimi, K. Davis, T. Tryfona, A. Liszka, H. Yates, J.A. London, A. Echevarría-Poza, J. Wurman-Rodrich, L. Yu, G. Thorlby, N. Spodsberg, K. R. Hanning, C. Fleischmann, X. Yu, K. Stott, K.B.R.M. Krogh, M. Sorieul, N. Anders, P. Dupree, GT61 β-1,2-xylosyltransferases define a conserved xylan modification in gymnosperm and Arabidopsis primary cell walls, Plant J. 124 (2025) e70545, https://doi.org/10.1111/TPJ.70545.

[50] M. Busse-Wicher, A. Li, R.L. Silveira, C.S. Pereira, T. Tryfona, T.C.F. Gomes, M. S. Skaf, P. Dupree, Evolution of xylan substitution patterns in gymnosperms and angiosperms: implications for xylan interaction with cellulose, Plant Physiol. 171 (2016) 2418–2431, https://doi.org/10.1104/pp.16.00539.

[51] G.J. Davies, K.S. Wilson, B. Henrissat, Nomenclature for sugar-binding subsites in glycosyl hydrolases, Biochem. J. 321 (Pt 2) (1997) 557–559. doi:https://doi.org/10.1042/BJ3210557.

[52] K. Tokuyasu, M. Mitsutomi, I. Yamaguchi, K. Hayashi, Y. Mori, Recognition of chitooligosaccharides and their N-acetyl groups by putative subsites of chitin deacetylase from a Deuteromycete, *Colletotrichum lindemuthianum*, Biochemistry 39 (2000) 8837–8843, https://doi.org/10.1021/BI0005355.

[53] M. Vardakou, J. Flint, P. Christakopoulos, R.J. Lewis, H.J. Gilbert, J.W. Murray, A family 10 *Thermoascus aurantiacus* xylanase utilizes arabinose decorations of xylan as significant substrate specificity determinants, J. Mol. Biol. 352 (2005) 1060–1067, https://doi.org/10.1016/J.JMB.2005.07.051.

[54] Y. Chu, T. Tu, L. Penttinen, X. Xue, X. Wang, Z. Yi, L. Gong, J. Rouvinen, H. Luo, N. Hakulinen, B. Yao, X. Su, Insights into the roles of non-catalytic residues in the active site of a GH10 xylanase with activity on cellulose, J. Biol. Chem. 292 (2017) 19315–19327, https://doi.org/10.1074/JBC.M117.807768.

[55] L. Lo Leggio, J. Jenkins, G.W. Harris, R.W. Pickersgill, X-ray crystallographic study of xylopentaose binding to *Pseudomonas fluorescens* xylanase A, Proteins Struct. Funct. Genet. 41 (2000) 362–373, https://doi.org/10.1002/1097-0134(20001115)41:3<362::AID-PROT80>3.0.CO;2-N.

[56] J. Sunseri, D.R. Koes, Pharmit: interactive exploration of chemical space, Nucleic Acids Res. 44 (2016) W442–W448, https://doi.org/10.1093/NAR/GKW287.

[57] R.A. Laskowski, J. Jabłońska, L. Pravda, R.S. Vařeková, J.M. Thornton, PDBsum: structural summaries of PDB entries, Protein Sci. 27 (2018) 129–134, https://doi.org/10.1002/PRO.3289.

[58] D. Krska, S. Mazurkewich, H.A. Brown, Y. Theibich, J.C.N. Poulsen, A.L. Morris, N. M. Koropatkin, L. Lo Leggio, J. Larsbrink, Structural and functional analysis of a multimodular hyperthermostable xylanase-glucuronoyl esterase from *Caldicellulosiruptor kristjansonii*, Biochemistry 60 (2021) 2206–2220, https://doi.org/10.1021/ACS.BIOCHEM.1C00305.

[59] J. Groen, A. Gazi, S. Kapishnikov, A. Brelot, M. Vos, J. Enninga, E. Pereiro, A. Sartori-Rupp, Cryo-CLXEM introduces cryo-SXT to bridge the resolution gap in cryo-CLEM, Communications Biology 2025 8:1 8 (2025) 1677-. doi:https://doi.org/10.1038/s42003-025-09072-x.